SPE/ISRM 47210

Stress Estimation in Faulted Regions: The Effect of Residual Friction

B. Wu, SPE, M. A. Addis, SPE, CSIRO Petroleum and N. C. Last, SPE, BP Exploration Colombia Ltd.

This paper was prepared for presentation at the SPE/ISRM Eurock '98 held in Trondheim, Norway, 8–10 July 1998.

Abstract

This paper presents relationships for estimating horizontal stresses based on the assumptions that the in situ stress state in a petroleum basin is controlled by the bounding normal or thrust faults at a limit equilibrium and that the fault block is linear elastic and plane strain condition applies in the direction parallel to the strike of the fault. These relationships are an extension of an earlier study and include the effect of residual friction angles on the estimation of horizontal stresses at depth.

The result shows that re-orientation of the minimum principal stress is possible after faulting depending on the Poisson's ratio of the formation. Predictions based on the relationships are compared with the stress data obtained in normal and thrust fault conditions as well as with the change in the minimum horizontal stress induced by the pore pressure depletion. The results show that to match the field stress data, a relatively low residual friction angle (10° - 30°) on the fault is required. This is further supported by the numerical modelling of the in situ stresses in the Cusiana field in Colombia, and is consistent with the residual friction angles measured in laboratory or back-calculated based on earthquake mechanism.

Introduction

A knowledge of in situ stresses at depth is essential for the design of drilling and completions for oil and gas wells, including well trajectory and mud weight selection, well casing design, and sand production and horizontal well stability prediction. Where the topographic surface in the area of interest is horizontal, it is generally accepted that the vertical stress is a principal stress and is equivalent to the total weight of the overburden. Determination of horizontal stresses is more complex, particularly the minimum horizontal stress and is the first obstacle to overcome in the quest for the knowledge of the in situ stresses at depth.

The standard leak-off test, routinely conducted to test casing shoes strength, is commonly used but inconsistently interpreted as an estimate of the minimum horizontal stress[1-4]. The test is normally performed two or three times in a well at the casing shoes, and they provide insufficient information about the changes of the stress within different lithologies, at different depths and at different stages of production. Indirect estimates of the in situ stresses is often required due to this paucity of reliable field measurements.

The elastic uniaxial strain model, based on a passive basin assumption, has been commonly used in estimations of the horizontal stresses. The predictions of the horizontal stress results from gravitational forces alone as the rock deformation is laterally constrained and no horizontal displacement occurs, under these conditions the horizontal stress is calculated as:

$$\sigma_h = \left(\frac{\nu}{1-\nu}\right)\sigma_v + p\left(\frac{1-2\nu}{1-\nu}\right) \qquad 1$$

where ν is the Poisson's ratio, p is the pore pressure and σ_v and σ_h are vertical and horizontal stresses respectively. By definition for the above boundary conditions, the two horizontal stresses are equal in magnitude (σ_h=σ_H). Variations in stresses in different lithologies are accounted for by using different Poisson's ratios for different rock types. However the Poisson's ratio has a theoretical value of less than 0.5, as such, a maximum principal stress oriented horizontally cannot be accounted for. Furthermore, faults bounding and compartmentalising reservoirs and breakouts in boreholes are commonly observed, indicting that the two horizontal stresses are not equal at depth. This makes the use of the passive basin assumption (Eq. 1) for stress estimations questionable.

Other methods and bases for horizontal stress estimation have been proposed, the main hypotheses are based on uniform strain applied horizontally to formations of varying stiffness, which enables stress contrasts in different lithologies to be accounted for. Secondly, failure based

hypotheses have been proposed for two conditions: the rock mass and the intact rock is at the point of limit equilibrium, or that stress is controlled by the weakest element in the rock mass - a favourable oriented and dominant fault, and the fault is at the point of limit equilibrium. These models are still relatively simple as they are monotonic loading models which cannot consider, analytically, stress rotations following the formation of the fault[5,6].

Reservoirs are commonly, if not invariably, bounded by faults. Seismic activities associated with production and water injection are recorded in a significant percentage of hydrocarbon producing basins[7,8], indicating active fault sliding. The stress changes to induce the seismic activity is typically small, approximately 1 MPa[9], implying that the stress state on the fault is at or near limit equilibrium. In a previous study[10], horizontal stresses are estimated based on a boundary condition of limit equilibrium on the normal and thrust faults, incorporating peak strength for fault friction which is only applicable when new faults are generated or when the fault residual friction and fault angle are consistent ($\alpha = 45\text{-}\phi'/2$, where ϕ' is fault residual friction angle).

This paper develops new analytical expressions for horizontal stress estimation by incorporating fault residual friction strength. The relation between stress state and fault angle is established. The effect of fault angles on the stress estimation is assessed. Conditions under which the stress state is affected by the fault are given. The paper will compare field measurements with the numerical results and the analytical expressions for the stresses acting at depth. Field stress conditions as well as the stress magnitudes can be satisfied using the analytical expressions with a range of fault angles and fault friction angles.

Horizontal Stress Estimation in Faulted Regions: Analytical Expression

Andersonian fault system. In Anderson's classification system, faults are classified as three "pure" types, i.e., normal, thrust and strike-slip[11]. It is assumed that one of the principal stresses is vertical and the other two are horizontal. Fault types are related to the magnitudes of the vertical and horizontal principal stresses. Normal faulting takes place when the maximum stress is in the vertical direction. A thrust fault is formed when the maximum principal stresses lies horizontally and the vertical stress is the minimum principal stress. For a strike-slip fault to take place, both maximum and minimum principal stresses must be horizontal and the vertical stress is the intermediate stress.

Fig.1 shows a simplified shear stress vs shear displacement relation on a fault plane during and after faulting. A fault is formed or re-activated when the shear stresses on the fault exceeds the shear strength of the formation or the fault. The shear strength may remain unchanged as represented by the dashed line, or may drop to the residual strength of the fault, as represented by the solid line. By assuming that the shear strength on the fault is unchanged, Addis et al[10] developed a set of stress equations for the prediction of horizontal stresses. Following a similar approach, this study focuses on the effect of decreasing shear strength characteristics of the fault zone resulting from the development of a residual friction at large deformations and the effect of this residual friction on horizontal stress estimation. In this study the stresses causing faulting or re-activation of a pre-existing fault are represented by the Mohr-Coulomb criterion.

Effect of fault angle on stress estimation. The normal and shear stresses (τ, σ_n)on a fault plane can be written as

$$\tau = \tfrac{1}{2}(\sigma_1 - \sigma_3)\sin 2\alpha$$
$$\sigma_n = \tfrac{1}{2}(\sigma_1 + \sigma_3) - \tfrac{1}{2}(\sigma_1 - \sigma_3)\cos 2\alpha \qquad 2$$

where α is the fault angle between the maximum principal stress and fault plane. The sliding condition on a pre-existing fault plane may be written as

$$\tau = \sigma_n' \tan\phi' \qquad 3$$

where $\sigma_n' = \sigma_n - p$.

Substituting Eq.2 into Eq.3 and re-arranging, the fault sliding condition can be expressed in terms of maximum and minimum principal stresses as

$$\frac{\sigma_3}{\sigma_1} = K_\alpha + (1 - K_\alpha)\frac{p}{\sigma_1} \qquad 4$$

where

$$K_\alpha = \frac{\sin(2\alpha + \phi') - \sin\phi'}{\sin(2\alpha + \phi') + \sin\phi'}$$

Fig.2 shows the effect of fault angle on the ratio of the minimum to maximum principal stresses as a function of fault angle. It is can be seen that the stress ratio reaches its maximum

$$\frac{\sigma_3}{\sigma_1}_{max} = \frac{1 - \sin\phi'}{1 + \sin\phi'} + \frac{2\sin\phi'}{1 + \sin\phi'}\frac{p}{\sigma_1} \qquad 5$$

when $\alpha = 45 - \phi'/2$, i.e., the fault is the weakest at this fault angle, hence maximum stress ratio is needed to maintain the fault in a stable condition. This fault angle is said to be consistent with the fault residual friction.

Conditions of sliding along a pre-existing fault. Limits on fault residual friction and fault angle exist for sliding along a pre-existing fault. For a given fault residual friction angle, sliding will take place only when the fault angle is within the range:

$$\frac{1}{2}\left[\arcsin\left(\frac{\sin\phi'}{\sin\phi}\right) - \phi'\right] < \alpha < \frac{1}{2}\left[180^o - \arcsin\left(\frac{\sin\phi'}{\sin\phi}\right) - \phi'\right] \qquad 6$$

in which stress state is effected by the existence of the fault. Outside the range, sliding cannot take place and the stress

state is controlled by the strength of rock formations rather than the fault strength. A new fault with a fault angle of $\alpha = 45 - \phi/2$ will be formed when the stress state is greater than the rock formation strength, where ϕ is the friction angle of intact rock.

For a given fault angle α, the maximum allowable fault residual friction angle can be expressed as:

$$\phi'_{max} < \arctan\left(\frac{\sin 2\alpha \sin\phi}{1-\cos 2\alpha \sin\phi}\right) \quad 7$$

for which fault sliding will take place on the pre-existing fault. When $\phi' > \phi'_{max}$ the fault has no effect on the stress state which is limited by the strength of rock formation.

Horizontal stress models based on residual friction of normal fault. Following the formation of a normal fault, the friction angle is reduced from that of intact rock to the residual friction angle on the fault plane/zone. Assuming that the maximum principal stress remains vertical and equal to the overburden, and the pore pressure is unchanged, from Eq.4 the normalised minimum horizontal stress acting on the fault can be expressed as:

$$\frac{\sigma_h}{\sigma_v} = K_\alpha + (1-K_\alpha)\frac{p}{\sigma_v} \quad 8$$

Note that for sliding along a newly formed fault, the fault angle is controlled by the friction angle of the intact rock. For subsequent sliding along a pre-existing fault, the fault angle and friction angle of intact rock may no longer be related to each other directly. The normalised minimum horizontal stress as a function of residual friction angle of the fault is plotted in **Fig.3**.

The maximum horizontal stress will be related to the stress conditions before as well as after a fault is formed. Assuming that the in situ stress state is defined by a passive basin condition before faulting (Eq.1), and that a plane strain condition may apply in the direction parallel to the strike of the fault during faulting and subsequent sliding - simulating a pure dip-slip motion on the fault - the stresses acting on the fault blocks can be estimated. It is further assumed that the faulted block acts in a linear elastic manner. The magnitude of the maximum horizontal stress can then be calculated as

$$\frac{\sigma_H}{\sigma_v} = \nu\left(1+K_\alpha\right) + \left[1-\nu(1+K_\alpha)\right]\frac{p}{\sigma_v} \quad 9$$

The ratio of the maximum to minimum horizontal stresses as a function of fault residual friction angle is plotted in **Fig.3**. Two stress regimes can exist after faulting, depending on the magnitudes of the Poisson's ratio. If

$$\nu \geq K_\alpha / (1+K_\alpha) \quad 10$$

is satisfied, the "pure" undisturbed normal fault stress condition is maintained, and the minimum horizontal stress is acting on the fault. For $\nu < K_\alpha / (1+K_\alpha)$, the minimum horizontal stress re-orientates in the direction parallel to the strike of the fault, i.e, normal to the plane strain boundary. The value of the Poisson's ratio separating the two stress regimes is 0.33, for a fault with a fault angle of 30° and a residual friction angle of 20°.

From Eqs.8 and 9, the ratio of the horizontal stresses can be expressed as

$$\frac{\sigma_H}{\sigma_h} = \frac{1}{K_\alpha}\left\{\nu\left(1+K_\alpha\right) + \left[K_\alpha - \nu(1+K_\alpha)\right]\frac{p}{\sigma_h}\right\} \quad 11$$

Eqs.9 and 11 are plotted as a function of pore pressure gradient in **Fig.4**. The anisotropy of the horizontal stresses depends on the magnitude of the pore pressure gradient. Over pressurizing leads to an increasingly isotropic stress state.

Horizontal stress models based on residual friction of thrust faults. For thrust fault conditions, the maximum and minimum principal stresses are the maximum horizontal and the vertical stresses, respectively. Following the formation of a thrust fault, the maximum and minimum horizontal stresses can be derived following a similar procedure to that applied to the normal fault condition. The magnitude of the maximum horizontal stress acting on the fault plane can be expressed as

$$\frac{\sigma_H}{\sigma_v} = K_\beta + (1-K_\beta)\frac{p}{\sigma_v} \quad 12$$

and the minimum horizontal stress as

$$\frac{\sigma_h}{\sigma_v} = \nu\left(1+K_\beta\right) + \left[1-\nu(1+K_\beta)\right]\frac{p}{\sigma_v} \quad 13$$

which is orientated in the direction parallel to the strike of the fault, where $K_\beta = 1/K_\alpha$. The normalised maximum and minimum horizontal stresses are plotted as a function of fault residual friction angle in **Fig.5** for a range of the Poisson's ratios.

Again, two stress regimes exist depending on the value of the Poisson's ratio, fault angle and fault residual friction angle. The horizontal dashed line in **Fig.5** defines the boundary between the two stress regimes. The "pure" thrust fault condition is maintained after faulting above the boundary. However, it becomes a strike-slip stress system blow the dashed line and both the maximum and minimum principal stresses lie in a horizontal plane. For a given fault angle and fault friction angle, $\sigma_h \geq \sigma_v$ when

$$\nu \geq 1/(1+K_\beta) \quad 14$$

is satisfied, i.e., a "pure" thrust fault stress condition is maintained. This corresponds to $\nu > 0.33$ for a fault angle of 30° and fault residual friction angle of 20°.

From Eqs.12 and 13 the horizontal stress ratio for "pure" dip-slip thrust deformation can be written as,

$$\frac{\sigma_H}{\sigma_h} = \frac{1}{\nu(1+K_\beta)}\left\{K_\beta - \left[K_\beta(1-\nu)-\nu\right]\frac{p}{\sigma_v}\right\} \qquad 15$$

The stress state defined in Eqs. 13 and 15 becomes increasingly isotropic with increasing in pore pressure gradient, an observation similar to that for a normal fault condition. This is purely a function of the use of frictional criterion on the fault planes, as the normal effective stresses diminish with increasing pore pressure, the differential stress to mobilise the fault decreases.

Comparison Between Stress models and Field Data

Eqs.8 to 15 developed in this study provide relationships between the three principal stresses based on boundary conditions of normal or thrust faults. The principal stresses are related to each other by a relationship based on fault residual friction and an assumption of plane strain condition in the direction parallel to the strike of the fault. The stress equations predict that the minimum principal stress can re-orientate by 90° for certain value of the Poisson's ratio, and the stress orientations associated with the three "pure" types of faults may no longer maintained after faulting.

A comparison between the model prediction and field data is required in order to assess the validity of the stress equations. Before estimates can be made for the horizontal stresses, the fault and formation properties must be known, including fault residual friction angle, fault angle in relation to the maximum principal stress and the Poisson's ratio of the formation. These data are rarely available. As such, the following examples are used to illustrate how these stress equations can be used to reproduce field stress data, when the input data are available or can be reasonably assumed.

It is interesting to note that the horizontal stress calculated using Eqs.8 to 15 are relatively insensitive to the choice of fault angle ranging from 20 to 40 degree. A change in fault angles from 20 to 40 degree causes a change in the calculated minimum horizontal stress less than 5% (normalised by the stress calculated at fault angle of 30°) for a fault residual friction angle of 15°, and this change decreases to 3.5% for a fault residual friction angle of 25°. A fault angle is related to the intact rock friction angle when the fault is newly formed. For a typical intact rock friction angle of 30 to 45°[12], the associated fault angle has a range of 30 to 22.5°. For the calculations described below, this range of fault angles are used in matching field stress data.

Two types of field data are analysed: the magnitudes of the minimum horizontal stresses and their response to pore pressure depletion.

In situ stress data, normal faults. Fig.6 shows the measured and calculated minimum horizontal stresses together with the back-calculated fault residual friction angle. The stress data are obtained from three areas as described below. They were selected because of relatively large number of high quality stress data and well defined rock properties.

Western Canadian Basin. Instantaneous shut-in and closure stresses were published from the records of over 100 minifrac tests conducted in Western Canadian basin[13]. Majority of the measurements were made in reservoir sandstones, some of which exhibited formation pressures that had been lowered by production. Many of the minimum horizontal stress data suggested a normal faulting stress boundary over much of the Alberta plains. However, higher values of the minimum horizontal stress were obtained from wells within or near the foothill of Rocky Mountains, due to existence of a thrust faulting stress regime[14]. The vertical stress is assumed to be 25kPa/m, equal to the overburden gradient[15]. The data obtained within or near the foothill of Rocky Mountains were excluded from analyses to avoid the uncertainties in the stress regime.

Measurements on core samples showed that the sandstones have a static Poisson's ratio of greater than 0.3[16]. Assuming that this value of the Poisson's ratio is representative of the sandstone formations in the basin, then a "pure" normal fault stress system is likely to be maintained after faulting for a fault residual friction angle of greater than 19° (Eq.10). The calculated minimum horizontal stress, Eq.8, based on these values is presented in **Fig.6**. A residual friction angle of 20 - 22° is required to "best" match the field stress data. Some large discrepancies exist between the stresses calculated from Eq.8 and measured. This is probably due to the fact the data set was obtained from a large area, and the stress state may not be controlled by a single normal fault (or a set of normal faults with similar fault properties).

East Texas basin. Stress measurements were made by conducting small volume hydraulic fracturing tests in GRI's SFE1, 2 and 3 wells in East Texas basin. The minimum horizontal stress data were obtained from an estimation of closure stresses[6]. The vertical stress is estimated to be 24 kPa/m and is the maximum principal stress. The tests were conducted in sandstone, mudstone and shale formations. But only the data obtained in the sandstone and mudstone formations are analysed in this study.

Both static and dynamic Poisson's ratios were measured on the preserved sandstone cores[6,17]. The sandstones have an average static and dynamic (saturated) Poisson's ratio of 0.17 and 0.23 respectively. The mudstone has a static Poisson's ratio of 0.27 - the dynamic Poisson's ratio is unavailable.

If the dynamic Poisson's ratio for sandstones and static one for mudstones are used in the analyses, a fault residual friction angle of 31° to 32° is required in order to "best" match the measured stress data. The minimum horizontal stress is predicted to be acting on the fault, which is consistent with the tensile and shear fractures observed in sandstone and mudstone cores[18].

DOE MWX site Colorado. Small volume hydraulic stress measurements (minifracs) were conducted at the US DOE's Multiwell Experiment (MWX) site to determined the

distribution of the minimum horizontal stress magnitudes with depth. The tests were conducted in sandstone and shale/siltstone/mudstone formations[19]. The minimum horizontal stresses were estimated from closure stress while the vertical stress was assumed to be equal to the weight of the overburden rocks. The average minimum horizontal to vertical stress ratio is approximately 0.85 in sandstone formations and approaches 1 in shale/mudstone formations.

Application of Eq.8 to the data set shows a fault residual friction angle in the range of 18 to 20°. The Poisson's ratios measured from sonic logs were 0.24 and 0.2 for shale/mudstone and sandstone formations respectively[19]. These values are lower than the Poisson's ratio required to maintain a "pure" normal fault stress system for the range of fault angles (22.5 to 30°). As such the minimum horizontal stress would be predicted to re-orientate to the direction parallel to the strike of the fault, i.e., on the plane strain boundary. Application of Eq.9 shows that a very low fault friction angle of 10 - 13° is required to "best" match the field stress data. Although some differences exist between the measured and calculated horizontal stresses, the model is able to predict the trend of the stress magnitudes in different lithologies (higher stress in shale/mudstone and lower stress in sandstone formations).

In situ stress data, thrust faults. Eq.14 predicts that for certain low values of Poisson's ratio re-orientation of the minimum principal stress by 90° is possible, and the stress system changes to "strike-slip" after faulting. The re-orientated minimum principal stress lies in a horizontal plane in a direction parallel to the strike of the fault and the vertical stress becomes the intermediate principal stress. This predicted stress system is consistent with the measurement in the Western Canadian foothills[13,14].

The minimum horizontal stress measured in the foothills has a magnitude of 0.92 ± 0.2 psi/ft, and is acting in a direction parallel to the structural trends of the fault planes. The vertical stress is the intermediate principal stress and has a gradient ranging 1.09 - 1.23 psi/ft. The maximum horizontal stress, acting on the fault, is the major principal stress and its gradient is 1.28 ± 0.48 psi/ft.

Assuming the pore pressure in the foothills is defined by a hydrostatic gradient, this thrust fault stress system can be satisfied with Poisson's ratio of 0.25 - 0.3, a fault residual friction angle of 10° and fault angle of 30°.

Depletion data. The passive basin assumption is most commonly used in predicting the minimum horizontal stress responses to variation in reservoir pressures. This is expressed as (from Eq.1):

$$\frac{\Delta\sigma_h}{\Delta p} = \left(\frac{1-2\nu}{1-\nu}\right) \qquad 16$$

The stress equation developed for normal and thrust fault conditions provided alternates to Eq.16. For a normal fault condition, a change in the ratio of the minimum horizontal stress to depletion may be expressed as:

$$\frac{\Delta\sigma_h}{\Delta p} = (1-K_\alpha) \qquad 17$$

for $\nu \geq K_\alpha/(1+K_\alpha)$ and

$$\frac{\Delta\sigma_h}{\Delta p} = \left[1-\nu(1+K_\alpha)\right] \qquad 18$$

for $\nu < K_\alpha/(1+K_\alpha)$;

For a thrust fault stress condition, a change in the ratio of the minimum horizontal stress to depletion may be expressed as:

$$\frac{\Delta\sigma_h}{\Delta p} = \left[1-\nu(1+K_\beta)\right] \qquad 19$$

for $\nu < 1/(1+K_\beta)$. For a Poisson's ratio less than this value, the vertical stress is the minimum principal stress and is not affected by the pore pressure depletion. The depletion relationships of Eqs.17 to 19 are presented in **Fig.7** as a function of fault residual friction angle and Poisson's ratio for both normal and thrust fault conditions. A wide range of depletion ratios from 0 to 1 is predicted.

Measurements of the minimum horizontal stress using hydraulic fracturing technique at different stages of production allow the changes of the minimum horizontal stress to be assessed as a function of reservoir pressures. Pore pressure depletion induced minimum horizontal stress changes and their effect on wellbore stability was discussed extensively by Addis[20,21]. Some of the field depletion data together with the Poisson's ratios for the fields are reproduced in Table 1.

The minimum horizontal stress responses to the pore pressure change are calculated using the Poisson's ratio derived for the fields based on passive basin assumption, Eq.16 and are presented in Table 1. A discrepancy exists between the calculated and measured depletion ratio. This could be caused by the choice of representative Poisson's ratio, as discussed by Addis et al[10], or due to incorrect assumption of passive basin.

Assuming that the stress fields in the reservoirs are controlled by active normal faulting, Eq.17 or 18 is used to match the filed data. For the given Poisson's ratios, the field depletion data can be closely matched by a fault residual friction angle of 19 - 23° for a fault angle range between 22.5 to 30°, with exception of Ekofisk field (Table 1). A high fault friction angle of 40 - 41 is required to match the Ekofisk data. The fault friction angle appears too high, in the range of expected value of intact formation friction strength. The discrepancy could be due to incorrect choice of Poisson's ratio or fault angle range but is more likely due to the structure of Ekofisk and the fact that the reservoirs has undergone

considerable compaction.

Horizontal Stress Estimation in Faulted Regions: Numerical Modelling

An example of the limitations of trying to estimate horizontal stresses by traditional methods is provided by the Cusiana[26,27] oil field in the Eastern Cordillera of Colombia, South America. The field is set in tectonically active foothills where the geology is characterised by high horizontal stresses, steeply dipping beds, numerous faults and alternating sand/shale sequences. The active deformation is dominated by movement on thrust faults. Many drilling difficulties were attributable to wellbore instability with hole sizes often exceeding two or even three times bit size. The conventional approach to addressing this requires at least a knowledge of the stress state and rock strengths so that theoretical stability calculations can be applied to calculate the range of mud weights which will maintain hole stability.

In this case, it soon became apparent that the stresses could not be estimated by traditional methods. In a true thrust regime, Andersonian fault mechanics predict the maximum principal stress to be horizontal and in the thrust direction, and the minimum to be vertical. However, the growing field evidence suggested that the minimum principal stress was horizontal and parallel to the mountain front - more representative in theory of a strike-slip setting. All subsequent information has confirmed this. How can this be explained? Indeed, it was this basic question that initially prompted the theoretical work described in this paper (and in Addis et al.[10]). Moreover, at the same time it was recognised that due to the complex structure of the area, the stress state was likely to vary spatially, and that to gain further insight into the wellbore instability issue, a more complete description of the stresses was desirable - something that the simpler analytical expressions were unlikely to yield. The likely variability of the stress field and the inability to characterise it completely by measurement - an operationally difficult and prohibitively expensive approach - led to the decision to gain an understanding of the stress field by computational stress analysis - a novel application of this established engineering tool.

The chosen modelling tool[28] incorporated the identified key structural features - the basic geometry, the faults (as discrete interfaces), the lithological contrasts and the current tectonic loading. The modelling was based on a series of two dimensional, plane strain, vertical cross sections corresponding to interpreted seismic lines through the Cusiana structure. Stress orientation determined from wellbore breakout analysis confirmed a very uniform direction for the maximum horizontal stress, which is consistent with the thrust direction, and with the assumption that the modelled section is a principal plane. The material was modelled in the simplest way that incorporates the main aspects of the mechanical behaviour of the system - intact rock as an elastic, Mohr Coulomb plastic solid, and the faults as simple frictional surfaces. After applying gravitational loading, representative tectonic boundary conditions were derived by laterally loading each model so as to mobilise (the right direction of) movement on the major faults. In other words, the modelling aim was to satisfy all geomechanical requirements (kinetic and kinematic) for an incremental displacement on the existing geometry - no attempt was made to reproduce the entire structural evolution. As such, computed solutions were expected to represent upper bounds to the stresses.

Intact rock properties were measured from core which showed typical measured peak friction angles of 20° and >40° for shales and sandstones, respectively. The friction angle of the faults was one of the variable parameters in the numerical models and was varied between 10° and 30°. To honour the geomechanical requirements and maintain consistency with the known geometry, the faults had to be much weaker than the intact rock - typically with friction angles of less than one half of the intact rock value; a fault friction angle of 18° was used to match the available field data in most of the models. A typical result, **Fig.8**, illustrates some important points which the simple analytical calculations presented in this paper cannot readily capture - for example, faults are rarely planar, and principal stresses can be rotated away from lithostatic (particularly near major faults), and the predicted stress magnitudes are inhomogeneous. The numerical modelling however also confirms some of the predictions from the simple analytical solutions, Eqs. 12 to 14, and confirms that under some circumstances, the principal stresses can re-orientate post-faulting so that the stress magnitudes would indicate a "strike-slip" regime, whereas in reality the kinematic constraint imposed by the existing fault geometries combined with the reduced fault strength determines the character of subsequent movements - thrust versus strike-slip. In this sense, the numerical modelling agreed with the simpler analytical predictions, and provided a potential key to understanding the Cusiana stress state.

The Friction Controlling Movement on Faults

The work to date has concentrated on the assumption that stresses acting in elastic rock masses bounded by faults can be defined by the strength of the fault planes or fault zones. The approach developed earlier[10] of a fault plane orientation which is consistent with the fault friction, has been expanded to differentiate between the fault orientation dictated by a rock mass peak friction angle and the subsequent residual friction angle which develops on the fault as a result of increasing deformation and fault gouge development[29].

In the comparison of the published field data and the predictions from the equations presented here, the orientation of the fault plane has been assumed, as this is rarely noted in publications, and the residual friction angle required to match the field measured stresses have been back-calculated. The

derived residual friction angles are in the range 10-30°: 20-22° for the Western Canadian Basin, 31-32° for the East Texas basin, 18-20° (10-13°) DOE MWX site Colorado, 10° for the Western Canadian foothills and 18° from the Cusiana numerical models. As these values are based on certain assumptions, the effective friction values likely to characterise fault sliding has been sought from other sources, as input to analytical expressions described in this paper for stress estimation.

The first reference that is normally quoted for frictional strengths of faults is the work undertaken by Byerlee[12] who collated the friction of a range of rock types reported in the open literature. The conclusion by Byerlee was that the expressions,

$$\tau = 0.85\sigma_n \qquad \text{for } \sigma_n \leq 200\text{MPa} \qquad 20$$

$$\tau = 0.5 + 0.6\sigma_n \qquad \text{for } \sigma_n > 200\text{MPa} \qquad 21$$

could describe the majority of frictional responses in intact rocks and rocks with finely ground surfaces. However, Byerlee states that faults normally contain gouge and that the frictional resistance of these faults will be "strongly dependent" upon the properties of the gouge, the values of which can be very low if comprised of clay minerals. Consequently, a maximum value for fault friction could be taken as 31° (friction coefficient = 0.6)[30].

A collation of residual friction angles and friction angles measured on fault gouge material measured in the laboratory and back calculated from fault movements[30,31] is presented in Table 2. The data comes from low stress tests but with large shear dispalcements[33,34], from high stress tests but in triaxial tests with characteristically low displacements [35,36,37] and from a back calculated value from analysis of field seismic events[38]. Table 2 shows that the range of friction angles from different sources point to values which are significantly lower than those represented by Eqs. 20 and 21. The friction angles typically vary from 4 to 39°, with the detailed values in the references tending to show values less than 20°: these residual friction angles would be obtained with material compositions exceeding 50% clay content[32,33]. The values presented in Table 2 do not all correspond to residual friction angles, which would be the large strain friction values which best represent the friction angle on a fault plane, as these are limited to the low stress results. However, the extrapolation of this residual friction angle data to high stress environments would normally lead to even lower values. These laboratory and field data tend to support the fault friction angles back-calculated in this study.

Another issue concerning the selection of the most appropriate fault friction angles to include in numerical and analytical models concerns the drainage state of the fault gouge. The tests results reported in Table 2 are friction angles measured during drained tests. The deformation along a fault will vary and can behave in a drained or undrained manner as the rate of deformation increases: the pore pressures generated during high deformation strain rates resulting from an "undrained shear". Such an undrained shear will lead to "self lubrication" of the fault surface and result in even lower apparent friction angles for the fault gouge than expected.

Conclusions

Relationships are established for the horizontal stresses based on assumptions that the in situ stress state in a petroleum basin is controlled by the bounding normal or thrust faults at a limit equilibrium and that the fault block is linear elastic and plane strain condition applies in the direction parallel to the strike of the fault. The horizontal stresses are estimated from the vertical stress, pore pressure and the mechanical properties on the fault plane and the rock formations. These relationships are an extension of an earlier study[10] and include the effect of residual friction angles on the estimation of horizontal stresses at depth.

The result shows that re-orientation of the minimum principal stress is possible after faulting depending on the Poisson's ratio of the formation. This re-orientation in the minimum principal stress direction is confirmed by the stress measurements in the thrust fault regions. Predictions based on the relationships are compared with the stress data obtained in normal and thrust fault conditions as well as with the change in the minimum horizontal stress induced by the pore pressure depletion. The results show that to match the field stress data, a relatively low residual friction angle (10° - 30°) on the fault is required. This is further supported by the numerical modelling of the Cusiana field in Colombia, a relatively structurally complex region, and is consistent with the residual friction angles measured in laboratory or back-calculated based on earthquake mechanism.

Caution should be taken in applying these relatively simple relationships in estimating the horizontal stresses. Further validation of the relationships is needed with well defined fault and formation mechanical properties, including the fault angle, and high quality in situ stress data.

NOMENCLATURE

σ_v = Vertical total stress, m/Lt^2, MPa
σ_H = Maximum horizontal total stress, m/Lt^2, MPa
σ_h = Minimum horizontal total stress, m/Lt^2, MPa
σ_n = Normal stress on the fault, m/Lt^2, MPa
τ = Shear stress on the fault, m/Lt^2, MPa
p = Pore Pressure, m/Lt^2, MPa
Δp = Pore pressure depletion, m/Lt^2, MPa
$\Delta\sigma_h$ = Min. horizontal stress change, m/Lt^2, MPa
ϕ = Internal friction angle of the intact rock, deg.
ϕ' = Residual friction angle of the fault, deg.
ϕ'_{max} = Max. residual friction angle of the fault, deg.
ν = Poisson's ratio

α = Angle of fault plane to σ_1, deg.
$\sigma_1 > \sigma_2 > \sigma_3$ = Principal stresses, m/Lt^2, MPa

SI Metric Conversion Factors

ft × 3.048* E-01 = m
psi × 6.894757 E+00 = kPa
*Conversion factor is exact.

References

1. Chenevert, M.E. and McLure, L. J.: "How to run casing and open-hole pressure tests". *The Oil and Gas Journal* (Mar. 1978), **76**, No. 10, 66.
2. Bell, J.S.: "The stress regime of the Scotian Shelf offshore eastern Canada to 6 kilometers depth and implications for rock mechanics and hydrocarbon migration". *Proc. Rock at Great Depth*, Pau (1990), **3**, 1243.
3. Breckels, I.M. and van Eekelen, H. A. M.: "Relationship between horizontal stress and depth in sedimentary basins", paper SPE 10336 presented at 56th Annual Conf., San Antonio, Texas (1981), 5-7 October.
4. Aadnoy, B.: *Modern Well Design*, John Wiley & Sons, A. A. Balkema, Rotterdam (1996).
5. Brace, W. F. and Kohlstedt, D. L.: "Limits on lithospheric stress imposed by laboratory experiments", *J. Geophy. Res.* (1980), **85**, No. B11, 6248.
6. Thiercelin, M.J. and Plumb, R. A.: "1991. A core-based prediction of lithological stress contrasts in east Texas formations", SPE 21847, *Rocky Mountain Regional Meeting and Low Permeability Reservoirs Symp.*, Denver, Colorado (1991), April 15-17, 429.
7. Grasso, J.-R.: "Mechanics of seismic instabilities induced by the recovery of hydrocarbons". *Pageoph.*(1992), **139**, No. 3/4, 507.
8. Segall, P.: "Earthquakes triggered by fluid extraction", *Geology* (1989), **17**, 942.
9. Segall, P.: "Induced stresses due to fluid extraction from axisymmetric reservoirs", *Pageoph* (1992), **139**, No. 3/4, 535.
10. Addis, M. A., Last, N. C. and Yassir, N. A.: "Estimation of horizontal stresses at depth in faulted regions and their relationship to pore pressure variations", *SPE Formation Evaluation* (March, 1996), 11.
11. Anderson, E. M.: *The dynamics of faulting, and dyke formation with applications to Britain*, Oliver and Boyd (1951).
12. Byerlee, J.: "Friction of Rocks". *Pure Appl. Geophysics* (1978), **116**, 615.
13. Woodland, D.C. & J.S. Bell, J. S.: "In situ stress magnitudes from mini-frac records in western Canada". *J. Canadian Petroleum Technology* (Sept.-Oct. 1989), **28**, No. 5, 22.
14. Woodland, D.C.: "Borehole instability in the western Canadian overthrust belt". *SPE Drilling Engineering* (March 1990), 27.
15. Caspillo, J. L.: "Modified fracture pressure decline analysis including pressure dependent leak off", *SPE paper 16417* (May 1987).
16. McLellan, P.: "In situ prediction and measurement by hydraulic fracturing, Wapiti, Alberta". *J. Can. Petrol. Tech.*(Mar. Apr., 1988), **27**, No.2, 85.
17. Walls, J. D. and Dvorkin, J.: "Measured and calculated horizontal stresses in the Travis Peak formation", *SPE Formation Evaluation* (Dec. 1994), 259.
18. Laubach, S. E.: "Subsurface fractures and their relationship to stress history in East Texas basin sandstone", *Tectonophysics* (1988), **156**, 37.
19. Warpinski, N. R.: "In situ stress measurements at US DOE's multiwell experiment site, Measverde group, Rifle, Colorado", *J. Petroleum Technology* (March 1985), 527.
20. Addis, M. A.: "Reservoir depletion and its effect on wellbore stability evaluation", *Int. J. Rock Mech. & Min. Sci.* (1997), **34**:3-4, Paper No. 004.
21. Addis, M. A., Hanssen, T-H, N. Yassir, D. Willoughby, and J. Enever.: "A comparison of leak-off tests and extended leak-off test data for stress estimation", *Proc. Eurock'98* (this volume).
22. Teufel, L. W., Rhett, D. W., and Farrell, H. E.: "Effect of reservoir depletion and pore pressure drawdown on in situ stress and deformation in the Ekofisk field, North Sea", *Proc. 32nd US Rock Mech. Symp., Rock Mechanics as a Multidisciplinary Science* (1991), Roegiers (ed.), Norman, Oklahoma, 63.
23. Ervine, W.B. and Bell, J. S.: "Subsurface in situ stress magnitudes from oil-well drilling records: an example from the Venture area, offshore eastern Canada". *Can. J. Earth Sci.* (1987), **24**, 1748.
24. Daines, S.R. "Prediction of fracture pressures for Wildcat wells". *J. Petroleum Technology* (April 1982), 863.
25. Whitehead, W. S., Hunt, E. R. and Holditch, S. A.: "The effects of lithology and reservoir pressure on the in situ stresses in the Waskom (Travis Peak) Field", *SPE/DOE 16403, Low Permeability Reservoir Symp.*, Denver, Colorado (May 1987), 139.
26. Addis, M.A., Last, N.C., Boulter, D. Roca-Ramisa, L., and Plumb, R. A.: "The quest for borehole stability in the Cusiana field, Colombia". *Oilfield Review* (April/July 1993), 33.
27. Last, N.C., Plumb, R.A., Harkness, R.M., Charlez, P., Alsen, J. and McLean, M.R.: "An Integrated Approach to Evaluating and Managing Wellbore Instability in the Cusiana Field, Colombia, South America". *SPE 30464* (1985).
28. Cundall, P.A. and Board, M.: "FLAC - a Microcomputer Program for Modelling Large-Strain Plasticity Problems". *Numerical Methods In Geomechanics, Proc. 6th Int. Conf.* (1988), Innsbruk, Balkema, Rotterdam.
29. Scholz, C.H.: "Wear and gouge formation in brittle faulting". *Geology* (June, 1987), **15**, 493.
30. Shimamoto, T.: " Rheology of rocks and plate tectonics". In. (ed. J. Hudson) *Comprehensive Rock Engineering*, Pergman press (1993), **1**, 93.
31. Hoek, E and Bray, J.W.: *Rock slope engineerin.* 3rd Ed., (1981), The Institution of mining and metallurgy, London.
32. Lupini, J.F., Skinner, A.E. and Vaughan, P.R.: "The drained residual strength of cohesive soils." *Geotechnique* (1981), **31**, No. 2, 181.
33. Skempton, A.W.: "Residual strength of clays in landslides, folded strata and the laboratory". *Geotechnique* (1985), **35**, No. 1, 3.
34. Börgesson, L., Broc, D. and Plas, F.: "Mechanical Properties of dense Ca-smectite clay". *Engineering Geology* (1990), **28** 419.
35. Moore, D. E., Lockner, D. A. Summers, R., Shengli, Ma and Byerlee, J.D.: "Strength of chrysotile-serpentinite gouge under hydrothermal conditions: can it explain a weak san Andreas fault?". *Geology* (Nov., 1996), **24**, No. 11, 1041.
36. Scott, D.R., Lockner, D.A. Byerlee, J. and Sammis, C.G.:

"Triaxial testing of Lopez Fault Gouge at 150 MPa Mean effective stress". *Pageoph,*(1994), **142**, No. 3/4, 749.
37. Chu, C.L., Wang, C.Y. and Lin, W.: "Permeability and frictional properties of San Andreas fault gouges". *Geophysical Research Letters*, **8**, No. 6, 565.
38. Iio, Y.: " Frictional coefficients on faults in a seismogenic region inferred from earthquake mechanism solutions". *Journal Geophysical Research* (1997), **102**, No. B3, 5403.

Table 1 Minimum stress vs pore pressure responses of fields and predicted responses

Field	$\Delta\sigma_3/\Delta p$	ν	*Eq.(17)*	ϕ'	*Eq.(18)*
Ekofisk[20]	0.8	0.33-0.38	0.75 - 0.5	40 - 41	0.78 - 0.8
Venture Field[21]	0.56	0.3	0.57	21 - 22	0.55 - 0.56
Waskom[22]	0.57	0.2-0.3	0.75 - 0.57	22 - 23	0.56 - 0.58
West Texas[23]	0.532	0.2-0.25	0.75 - 0.67	19 - 21	0.532
Wytch Farm[19]	0.55	0.21	0.73	20 - 22	0.55

Table 2 Residual friction values for faults and discontinuities.

Ref.	*Gouge Type*	*Residual Friction Angle*	*Residual/Fault Friction Friction Coefficient*	*Friction Value Source*	*Stress range*
30	*Clay*	11.3°	0.2	Mechanical test	Low Stress range
31	*Various*	8.5-25°	0.15-0.47	Filled Discontinuities	
32	*Sand-bentonite*	4-30.5°	0.589-0.075	Mechanical test	Low <1 MPa
32	*Happisburgh - London clay*	6-33°	0.640-0.107	Mechanical test	Low <1 MPa
32	*sand-mica*	15-30°	0.573 - 0.277	Mechanical test	Low <1 MPa
32	*Various*	7.0°-39°	0.122-0.81	Mechanical test	Low <1 MPa
33	*Clays <25%*	>20°	>0.364	Mechanical test	Low <1 MPa
33	*Clays >50%*	5-15°	0.087-0.267	Mechanical test	Low <1 MPa
33	*Ca -smectite**	4-10°	0.07-0.18	Mechanical test	1-10 MPa
35	*Chrysotile**	6-27°	0.1-0.5	Mechanical test	100MPa
36	*Lopez Fault**	22-31°	0.4-0.6	Mechanical test	150MPa
37	*San Andreas Fault**	14°	0.25	Mechanical test	200MPa
38	*Kinki district*	11.3°	≤0.2	Earthquake mechanisms	-

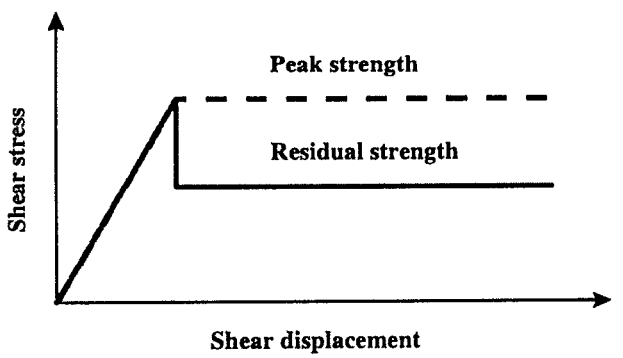

Fig.1-Simplified shear stress vs shear displacement behaviour.

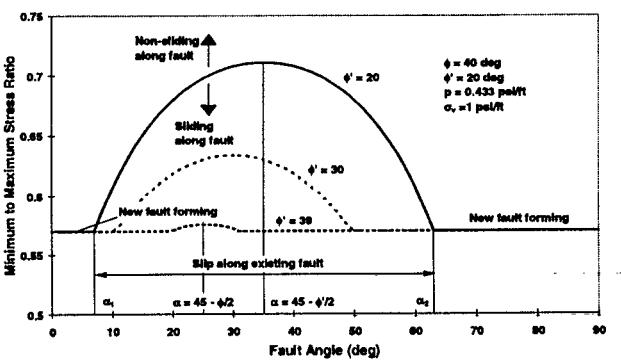

Fig.2-Effect of fault angle on the minimum to maximum stress ratio.

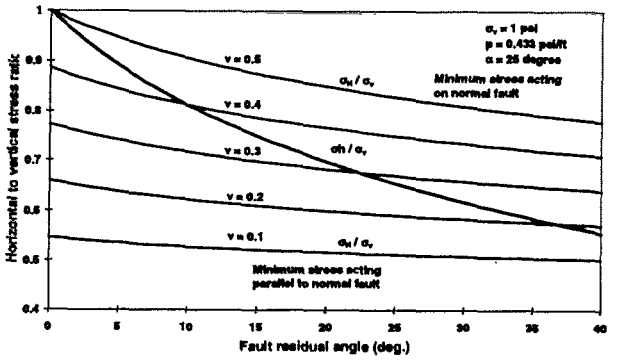

Fig.3-Fault-parallel horizontal stress as a function of fault friction: Normal faulting.

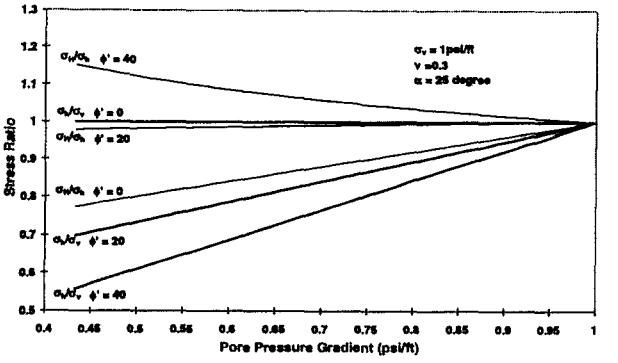

Fig.4-Stress ratio as a function of pore pressure gradient, normal faulting.

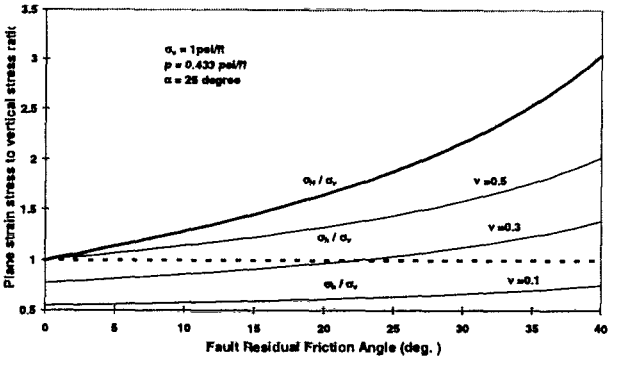

Fig.5-Ratio of horizontal to vertical stress as a function of fault residual friction angle, thrust fault condition.

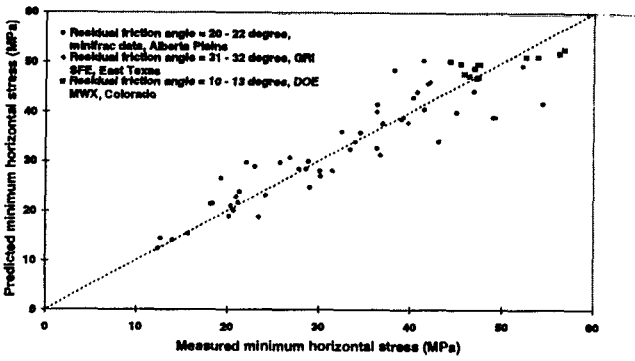

Fig.6-Scatter plot of measured and calculated minimum horizontal to vertical stress ratio, normal faulting.

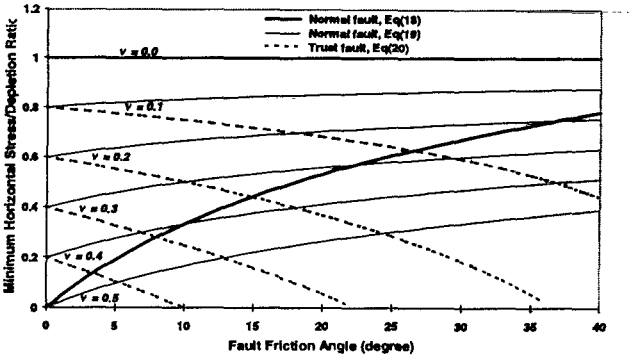

Fig.7-Minimum horizontal stress to pore pressure depletion ratio as a function of fault residual friction angle, normal and thrust faulting.

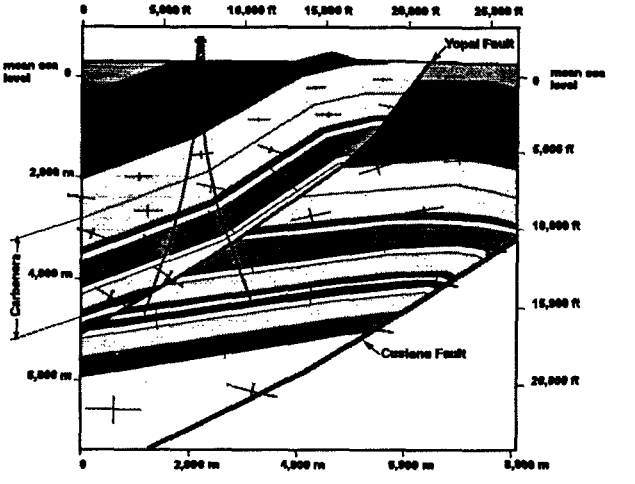

Fig.8-Typical result from numerical modelling of a section through the Cusiana field showing the fault geometries, lithological contrasts and predicted in plane stresses (as tensors)